TU Delft

Delft University of Technology

Isogeometric solution of helmholtz equation with dirichlet boundary condition in regions with irregular boundary

Numerical experiences

Mederos, Victoria Hernández; Ugalde, Isidro Abelló; Alfonso, Rolando M.Bruno; Lahaye, Domenico; Ones, Valia Guerra

DOI
10.4208/ijnam2023-1001

Publication date
2023

Document Version
Final published version

Published in
International Journal of Numerical Analysis and Modeling

Citation (APA)
Mederos, V. H., Ugalde, I. A., Alfonso, R. M. B., Lahaye, D., & Ones, V. G. (2023). Isogeometric solution of helmholtz equation with dirichlet boundary condition in regions with irregular boundary: Numerical experiences. *International Journal of Numerical Analysis and Modeling*, *20*(1), 1-28. https://doi.org/10.4208/ijnam2023-1001

Important note
To cite this publication, please use the final published version (if applicable).
Please check the document version above.

Copyright
Other than for strictly personal use, it is not permitted to download, forward or distribute the text or part of it, without the consent of the author(s) and/or copyright holder(s), unless the work is under an open content license such as Creative Commons.

Takedown policy
Please contact us and provide details if you believe this document breaches copyrights.
We will remove access to the work immediately and investigate your claim.

This work is downloaded from Delft University of Technology.
For technical reasons the number of authors shown on this cover page is limited to a maximum of 10.

Green Open Access added to TU Delft Institutional Repository

'You share, we take care!' - Taverne project

https://www.openaccess.nl/en/you-share-we-take-care

Otherwise as indicated in the copyright section: the publisher is the copyright holder of this work and the author uses the Dutch legislation to make this work public.

INTERNATIONAL JOURNAL OF
NUMERICAL ANALYSIS AND MODELING
Volume 20, Number 1, Pages 1–28

© 2023 Institute for Scientific
Computing and Information
doi: 10.4208/ijnam2023-1001

ISOGEOMETRIC SOLUTION OF HELMHOLTZ EQUATION WITH DIRICHLET BOUNDARY CONDITION IN REGIONS WITH IRREGULAR BOUNDARY: NUMERICAL EXPERIENCES

VICTORIA HERNÁNDEZ MEDEROS, ISIDRO ABELLÓ UGALDE, ROLANDO M. BRUNO ALFONSO, DOMENICO LAHAYE, AND VALIA GUERRA ONES

Abstract. In this paper we use the Isogeometric Analysis (IgA) to solve the Helmholtz equation with Dirichlet boundary condition over a bounded physical 2D domain. Starting from the variational formulation of the problem, we show how to apply IgA to obtain an approximated solution based on biquadratic B-spline functions. We focus the attention on problems where the physical domain has very irregular boundary. To solve these problems successfully a high quality parametrization of the domain must be constructed. This parametrization is also a biquadratic tensor product B-spline function, with control points computed as the vertices of a quadrilateral mesh with optimal geometric properties. We study experimentally the influence of the wave number and the parametrization of the physical domain in the accuracy of the approximated solution. A comparison with classical Finite Element Method is also included. The power of IgA is shown solving several difficult model problems, which are particular cases of the Helmholtz equation and where the solution has discontinuous gradient in some points, or it is highly oscillatory. For all model problems we explain how to select the knots of B-spline quadratic functions and how to insert knew knots in order to obtain good approximations. The results obtained with our implementation of the method prove that IgA approach is successful, even on regions with irregular boundary, since it is able to offer smooth solutions having at the same time some singular points and high number of oscillations.

Key words. Isogeometric analysis, Helmholtz equation, irregular regions.

1. Introduction

In its most general form Helmholtz equation in 2D is given by

$$-\Delta u(x,y) - k^2(x,y)u(x,y) = f(x,y), \quad (x,y) \in \Omega, \tag{1}$$

where $k(x,y)$ and $f(x,y)$ are known functions and Δ denotes the Laplacian operator.

Due to its importance in different fields such as acoustic and electromagnetic systems, the case k equal to a positive constant have been intensively investigated over the years, see for instance [23], [24], [14], [29]. In this case, $u(x,y)$ is the amplitude of a wave traveling along Ω and k, called wave number, is the number of waves per unit of distance. The more complicated scenario, where $k(x,y)$ is a function depending on spatial variables, is also important. For instance, the wave function that satisfies a Schrödinger equation model of two interacting atoms [28] is solution of a Helmholtz equation with variable $k(x,y)$. Moreover, in realistic geophysical applications [16], $u(x,y)$ is the pressure wavefield and $k(x,y) = \omega^2/(\rho c^2)$, where ω is the angular frequency, $c = c(x,y)$ is the wave propagation velocity of the medium and $\rho = \rho(x,y)$ is the mass density, and both, $c(x,y)$ and $\rho(x,y)$ can contain high-contrast variations in space.

Received by the editors on July 20, 2021 and, accepted on August 30, 2022.
2020 *Mathematics Subject Classification.* 35J05, 65N30.

If k is a small constant, Helmholtz equation can be solved successfully using low degree p *Finite Element Method* (FEM). But as k is increased, the number N_{FEM} of degrees of freedom necessary to obtain an accurate approximation of $u(x, y)$ must be proportional to k^2 [17], or the mesh size h have to be selected in such a way that $hk^{(p+1)/p}$ is constant and sufficiently small [27]. Moreover, many numerical difficulties appear [27], [14], [29], [17], [12]. These difficulties are associated with the fact that the standard variational formulation of the Helmholtz equation is sign-indefinite, hence for k sufficiently large, the coefficient matrix is indefinite and non-normal. As a consequence, iterative methods to solve the corresponding linear systems with N_{FEM} unknowns require the use of preconditioners, such as multigrid methods, domain decomposition, complex shifted Laplacian and deflation, see for instance [13], [32], [11].

Isogeometric analysis (IgA) was introduced by Hughes et al. in [21] as an extension of FEM to solve partial differential equations (PDE). The term *isogeometric* highlights that IgA uses B-splines functions twice: to parametrize Ω and as shape functions to approximate the solution of the PDE. In IgA approach B-splines functions may be constructed to have high smoothness. This is very important for problems with smooth solutions, where in comparison with FEM, IgA provides improved accuracy per degree of freedom. The first step to solve a PDE with IgA is the parametrization of Ω. This is currently an active research area, see for instance [34], [35], [30], [20], [36], [15], [31], [37] and [1]. The parametrization of the physical domain avoids the small errors introduced by FEM mesh, which can be amplified significantly in the context of wave propagation problems. In the last years IgA approach has been successfully used for a wide variety of PDE applications, see [3], [38], [6].

Previous work

Several recent papers [7], [9], [10], [12], adopted IgA as discretization technique to solve the Helmholtz equation with different boundary conditions. In [7] Helmholtz equation with Neumann boundary condition is solved in a domain described by 4 quadratic B-spline curves. Moreover, the acoustic in the interior of a simplified 2D model of a car is studied, for a wide frequency range. This problem is modeled with Helmholtz equation with Robin and Neumann boundary conditions. The results of the experiments in this paper confirm that, for similar degrees of freedom, IgA manage acoustic problems more efficiently than FEM, since it suffers less of the pollution errors, specially in the higher frequency range. In [9] partition of unity isogeometric analysis is applied for computing the scalar acoustic potential, governed by Helmholtz equation subject to (complex) Robin boundary condition. The study is focused in a comparison between FEM and IgA, including the use of enriched basis functions to reduce the pollution and also to avoid the need for domain re-meshing at high frequencies. The paper concludes that IgA has a clear advantage over FEM, since it achieves similar errors with significantly less degrees of freedom.

The numerical solution of the linear system derived from IgA discretization of Helmholtz equation is the central topic of papers [10] and [12]. In [10], Helmholtz equation is solved with Robin boundary condition. The performance of GMRES is investigated in the context of IgA, and it is compared to FEM, especially at high polynomial orders. The study includes the use of preconditioners such as ILU with a complex shift and complex shifted Laplacian. The conclusion is that to reach the convergence of GMRES, IgA needs fewer iterations compared to FEM. In [12],

Helmholtz equation is considered on a square domain with homogeneous Dirichlet boundary condition. The linear system is solved with GMRES and its convergence is accelerated with a deflation technique, based on rational quadratic Bezier curves. The deflation scheme is combined with the approximated inverse of the Complex Shifted Laplacian Preconditioner, computed with a multigrid method. Numerical results are shown, confirming scalable convergence with respect to the wave number and the order of the B-spline basis functions.

The problem and our contribution

In this paper we apply the isogeometric approach to solve the Helmholtz equation (1) over a bounded physical domain Ω, with Lipschitz continuous boundary Γ and nonhomogeneous Dirichlet boundary condition

$$u(x,y) = g(x,y), \quad (x,y) \in \Gamma. \tag{2}$$

We are specially interested in problems where the physical regions Ω has a very irregular boundary, such as lagoons, lakes, islands, etc. In this regard, the problem treated here is different from the ones studied in [7], [9], [10] and [12], since they deal with very simple domains, like circles or squares, or with closed domains with simple boundary curves. In consequence, the construction of the parametrization of Ω is qualitatively more complex in our case. To obtain a high quality parametrization, we use a biquadratic tensor product B-spline, computed by the method proposed in [1]. For complex domains, the quality of the parametrization is very important, since it has an strong influence on the speed of convergence of the approximated solution and also on the condition number of the discretization matrix [35], [31]. Frequently, the quality of the parametrization is evaluated using several measures, but the ultimate quality criterion is the accuracy of the approximated solution obtained using a given parametrization. In this sense, one goal of the present paper is to show that indeed the parametrization method proposed in [1] can be successfully used to solve Helmholtz equation with Dirichlet boundary condition over domains with irregular boundary.

Another difference between our work and the previous ones is that we prescribe Dirichlet boundary condition. In contrast, Robin boundary condition is considered in [9] and [10], while [7] works with Neumann or Robin and Neumann boundary conditions. Only [12] fixes Dirichlet homogeneous boundary condition, but in that case the domain is the unit square. In this sense, it is important to notice that in comparison with other boundary conditions, the solution of Helmholtz equation with Dirichlet boundary condition is more challenging, since the corresponding linear system exhibits the distribution of the eigenvalues that is most unfavorable for the convergence of Krylov-type iterative solvers [18].

The main contribution of our paper is a complete methodology to apply isogeometric analysis for the solution of Helmholtz equation with Dirichlet boundary condition on 2D closed regions with very irregular boundary. This methodology is based in the method proposed in [1] to obtain good parametrizations of complex domains. To show the success of the method, we solve several difficult model problems, obtained as particular cases of the Helmholtz equation. The first model problem is the Poisson equation with a right hand side function $f(x,y)$, defined in such away that the exact solution is a function with discontinuous gradient in three points. The second model problem is a Helmholtz equation with constant wave number k and a highly oscillatory solution $u(x,y)$. For this problem we study

the influence of the wave number k and the parametrization of the physical domain in the quality of approximated solution computed with IgA. We also compare this solution with the approximation obtained using classical FEM, showing that even when the L^2 and H^1 errors of IgA and FEM approximated solutions are of the same order, the computational cost of FEM is higher, since it requires more degrees of freedom than IgA to obtain these errors. In the last model problem we study a Helmholtz equation, where the wave number $k(x, y)$ depends of spatial variables, and the exact solution is highly oscillatory near a singular point. For all model problems we show how to construct the sequence of knots of the biquadratic B-spline functions, in order to obtain approximations of the exact solution, having a behavior similar to the exact solution, including singular points and oscillations. The performance of our implementation to solve the previous problems in several regions with very irregular boundary is also included, proving that the method produces accurate approximations to the exact solution.

Organization of the paper

The paper is organized as follows. In section 2 we obtain the variational formulation of Helmholtz equation with nonhomogeneous Dirichlet boundary condition. The isogeometric method is described in section 3, using biquadratic B-spline functions to approximate the solution of the problem. Details about the basic steps of the method are given in this section, including the obtention of the linear system of equations, which provides the coefficients of the approximated solution written in the tensor product B-spline basis. Section 4 describes how to approximate the Dirichlet boundary condition. Moreover, computational aspects of the assembly process are also given. In section 5 we show how to apply the IgA approach to the solution of several model problems that are particular cases of the Helmholtz equation defined on physical regions with irregular boundary. Section 6 concludes the paper.

2. Variational formulation.

FEM and IgA have both the same theoretical basis, namely the weak or variational formulation of a PDE. In this section we obtain the variational formulation of Helmholtz equation with homogeneous boundary condition. Our problem with boundary condition (2) is reduced to a problem with homogeneous boundary condition writing the solution of (1) as

$$u(x, y) = u_0(x, y) + u_g(x, y), \tag{3}$$

where the function u_0 satisfies (1) and

$$u_0(x, y) = 0, \quad \text{for } (x, y) \in \Gamma, \tag{4}$$

while

$$u_g(x, y) = g(x, y), \quad \text{for } (x, y) \in \Gamma. \tag{5}$$

Thus, substituting (3) in (1) we transform the original problem (1)-(2) into the following problem with homogeneous Dirichlet boundary condition

$$-\Delta u_0(x, y) - k^2(x, y)u_0(x, y) = \widetilde{f}(x, y), \tag{6}$$

where $\widetilde{f}(x, y) = f(x, y) + \Delta u_g(x, y) + k^2(x, y)u_g(x, y)$. Let $\mathcal{V}$ the Hilbert space of functions

$$\mathcal{V} = \{v \in H^1(\Omega) \ / v(x, y) = 0 \text{ for } (x, y) \in \Gamma\}, \tag{7}$$

which consists of all functions $v \in L^2(\Omega)$ that possess weak and square-integrable first derivatives and that vanish on the boundary. The norm $\|v\|_{\mathcal{V}}$ in this space is given by

$$\|v\|_{\mathcal{V}}^2 = \int\int_{\Omega} v^2 + \left(\frac{\partial v}{\partial x}\right)^2 + \left(\frac{\partial v}{\partial y}\right)^2 \, d\Omega. \tag{8}$$

To obtain the variational formulation we multiply (6) by $v \in \mathcal{V}$ and integrate on Ω

$$\int\int_{\Omega} (-\Delta u_0(x,y) - k^2(x,y)u_0(x,y))v(x,y) \, d\Omega = \int\int_{\Omega} \widetilde{f}(x,y)v(x,y) \, d\Omega. \tag{9}$$

Using the Green formula in (9) and taking into account that $v \in \mathcal{V}$ we obtain the variational formulation of problem (6): find $u_0 \in \mathcal{V}$ such that for all $v \in \mathcal{V}$

$$a(u_0, v) = G(v), \tag{10}$$

where $a(u,v)$ is the bilinear form

$$a(u,v) = \int\int_{\Omega} (\nabla u(x,y)^t \nabla v(x,y) - k^2(x,y)u(x,y)v(x,y)) \, d\Omega, \tag{11}$$

and $G(v)$ is the linear form

$$G(v) = \int\int_{\Omega} (f(x,y) + k^2(x,y)u_g(x,y))v(x,y) \, d\Omega - \int\int_{\Omega} \nabla u_g(x,y)^t \nabla v(x,y) \, d\Omega. \tag{12}$$

The existence and uniqueness of weak solution has been very well studied when $k(x,y)^2 = \lambda$, where λ is a real constant, see for instance [33]. For $\lambda = 0$ the bilinear form $a(u,v)$ given by (11) is *coercive*. Therefore, Lax-Milgram theorem guarantees the existence and uniqueness of a solution to the variational problem (10) and the continuous dependence of the solution on the data. On the other hand, if $\lambda = \lambda_j$, where λ_j is the j-th Dirichlet eigenvalue of the negative Laplacian in Ω, i.e. there exists a $u_j \in H^1(\Omega) \setminus 0$ such that $-\Delta u_j = \lambda_j u_j$ in Ω and $u_j = g$ on Γ, then the problem has solution but it is not unique. Finally, if λ is not an eigenvalue of the negative Laplacian, then the bilinear form $a(u,v)$ satisfies a Gärding inequality and again the variational problem (10) has a unique solution which depends continuously on f.

There are few results in the literature about the Helmholtz equation with variable coefficient $k(x,y)$. In the recent paper [19], existence and uniqueness results for this problem are obtained under rather general conditions on the function $k(x,y)$, using the unique continuation principle and the Fredholm alternative.

3. Galerkin method with isogeometric approach.

The Galerkin method solves the variational problem assuming that the approximated solution belongs to a finite-dimensional subspace $\mathcal{V}_h$. In the classical FEM, $\mathcal{V}_h$ consists of piecewise polynomials functions with global C^0 continuity. This space is defined in terms of a partition of the physical domain Ω in a mesh of triangles or quadrilaterals. In the isogeometric approach [8], the subspace $\mathcal{V}_h$ is generated by tensor product B-spline functions (or more general by NURBs functions) with higher global continuity.

3.1. Parametrization of the domain. In order to solve a PDE using isogeometric analysis a suitable parametrization of the physical domain Ω is required. Assuming that Ω is topologically equivalent to the unit square $\hat{\Omega}$, its boundary can be divided into 4 curves in such a way that consecutive curves are the image by the *unknown* parametrization

$$\mathbf{F}(\xi,\eta) : \hat{\Omega} \longrightarrow \Omega,$$

of consecutive sides of $\hat{\Omega}$. In this paper, we assume that $\mathbf{F}(\xi,\eta)$ is an *injective biquadratic B-spline* function that can be written as [4]

$$\mathbf{F}(\xi,\eta) = (x(\xi,\eta), y(\xi,\eta))^t = \sum_{i=1}^{n}\sum_{j=1}^{m} \mathbf{P}_{i,j} B^3_{i,t^\xi}(\xi) B^3_{j,t^\eta}(\eta), \tag{13}$$

where $\mathbf{P}_{i,j} = (P^x_{i,j}, P^y_{i,j})^t,\ i = 1,...,n,\ j = 1,...,m$ are the *control points*, $B^3_{i,t^\xi}(\xi)$ is the i-th quadratic B-spline for the knot sequence t^ξ and $B^3_{j,t^\eta}(\eta)$ is the j-th quadratic B-spline for the knot sequence t^η with

$$t^\xi = (0,0,\xi_1,\xi_2,...,\xi_{n-1},1,1), \quad 0 = \xi_1 < \xi_2 < ... < \xi_{n-1} = 1, \tag{14}$$

$$t^\eta = (0,0,\eta_1,\eta_2,...,\eta_{m-1},1,1), \quad 0 = \eta_1 < \eta_2 < ... < \eta_{m-1} = 1. \tag{15}$$

In other words, $\mathbf{F}(\xi,\eta)$ is a function in the tensor product space $\mathbb{S}_{3,t^\xi} \bigotimes \mathbb{S}_{3,t^\eta}$, where $\mathbb{S}_{3,t}$ denotes the space of quadratic spline functions for the knot sequence t. The space $\mathbb{S}_{3,t^\xi} \bigotimes \mathbb{S}_{3,t^\eta}$ has dimension $n \times m$.

We assume that Γ is composed by two *quadratic B-splines curves*, $\mathbf{F}(\xi,0)$, and $\mathbf{F}(\xi,1),\ 0 \leqslant \xi \leqslant 1$, both with knots t^ξ and two *quadratic B-splines curves*, $\mathbf{F}(0,\eta)$, and $\mathbf{F}(1,\eta),\ 0 \leqslant \eta \leqslant 1$, both with knots t^η. It means that by hypothesis, boundary control points of the map $\mathbf{F}$: $\mathbf{P}_{i,1}, \mathbf{P}_{i,m},\ i = 1,...,n$ and $\mathbf{P}_{1,j}, \mathbf{P}_{n,j},\ j = 1,...,m$ are known. In consequence, the parametrization problem is reduced to compute the *internal* control points. Denote by $\Omega^{'}$ the planar region whose boundary is the polygonal made up by the boundary control points of the map $\mathbf{F}$. The interior control points $\mathbf{P}_{i,j}$, $i = 2,...,n-1$, $j = 2,...,m-1$ are computed as the inner vertices of a *structured quadrilateral mesh* G on $\Omega^{'}$. These vertices are obtained minimizing a functional that measures some geometric properties of G. For more details about the computation of the control points see [1], where necessary and sufficient conditions for the injectivity of the map $\mathbf{F}(\xi,\eta)$ are also studied. Figure 1 shows the quadratic B-splines boundary curves and the control mesh of the biquadratic map $\mathbf{F}$ parametrizing Havana bay region.

3.2. Galerkin method. To simplify the notation, in the rest of the paper we don't write the subindex t^ξ or t^η of the B-spline functions when it is clear from the context. The functions

$$B^3_{i,j}(\xi,\eta) := B^3_i(\xi) B^3_j(\eta),\ \ i = 1,...,n,\ \ j = 1,...,m, \tag{16}$$

define a basis of $\mathbb{S}_{3,t^\xi} \bigotimes \mathbb{S}_{3,t^\eta}$. Moreover, due to the assumptions on the parameterization $\mathbf{F}$, the functions

$$\phi_{i,j}(x,y) := (B^3_{i,j}\, o\, \mathbf{F}^{-1})(x,y),\ \ i = 1,...,n,\ \ j = 1,...,m, \tag{17}$$

are independent in Ω. With the help of $\mathbf{F}$, integrals (11),(12) over Ω can be transformed into integrals over $\hat{\Omega}$ by means of the integration rule

$$\int\int_{\Omega} w(x,y)\, d\Omega = \int_0^1 \int_0^1 w(\mathbf{F}(\xi,\eta))\, |\det J\mathbf{F}(\xi,\eta)|\ d\xi\, d\eta,$$

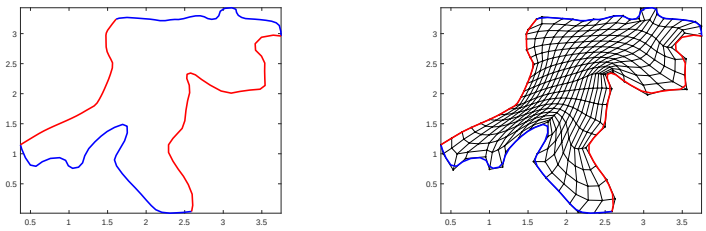

FIGURE 1. Left: Havana bay region Ω. Blue curves: "south" and "north" quadratic B-spline curves $\mathbf{F}(\xi,0)$ and $\mathbf{F}(\xi,1)$ respectively. Red curves: "west" and "east" quadratic B-spline curves $\mathbf{F}(0,\eta)$ and $\mathbf{F}(1,\eta)$ respectively. Right: boundary curves and the control mesh of $\mathbf{F}(\xi,\eta)$ with $n \times m = 1\,444$ points, $n = 38$ and $m = 38$.

where $J\mathbf{F}$ denotes the Jacobian matrix of the parametrization

$$J\mathbf{F}(\xi,\eta) = \begin{pmatrix} \partial x/\partial\xi & \partial x/\partial\eta \\ \partial y/\partial\xi & \partial y/\partial\eta \end{pmatrix}. \tag{18}$$

Applying the chain rule to the function $w(x,y) = w(\mathbf{F}(\xi,\eta))$ we obtain

$$\nabla_{(x,y)} w(x,y) = J\mathbf{F}(\xi,\eta)^{-t} \nabla_{(\xi,\eta)} w(\xi,\eta), \tag{19}$$

where the notation $\nabla_{(x,y)}$ means that partial derivatives are computed with respect to variables x, y and $J\mathbf{F}(\xi,\eta)^{-t}$ denotes the transpose of the inverse of $J\mathbf{F}(\xi,\eta)$. Hence, integrals (11),(12) defining the weak formulation can be written as

$$\begin{aligned} a(u,v) &= \int_0^1 \int_0^1 (J\mathbf{F}(\xi,\eta)^{-t} \nabla_{(\xi,\eta)} u)^t (J\mathbf{F}(\xi,\eta)^{-t} \nabla_{(\xi,\eta)} v) \, |\det J\mathbf{F}(\xi,\eta)| \, d\xi d\eta \\ &- \int_0^1 \int_0^1 k^2(\mathbf{F}(\xi,\eta)) u(\mathbf{F}(\xi,\eta)) v(\mathbf{F}(\xi,\eta)) \, |\det J\mathbf{F}(\xi,\eta)| \, d\xi \, d\eta, \end{aligned} \tag{20}$$

and

$$\begin{aligned} G(v) &= \int_0^1 \int_0^1 (f(\mathbf{F}(\xi,\eta)) + k^2(\mathbf{F}(\xi,\eta)) \, u_g(\mathbf{F}(\xi,\eta))) v(\mathbf{F}(\xi,\eta)) | \det J\mathbf{F}(\xi,\eta)| d\xi d\eta \\ &- \int_0^1 \int_0^1 (J\mathbf{F}(\xi,\eta)^{-t} \nabla_{(\xi,\eta)} u_g(\xi,\eta))^t J\mathbf{F}(\xi,\eta)^{-t} \nabla_{(\xi,\eta)} v(\mathbf{F}(\xi,\eta)) | \det J\mathbf{F}(\xi,\eta)| d\xi d\eta. \end{aligned} \tag{21}$$

The approximated solution $u_0^h(x,y)$ is sought in the space

$$\mathcal{V}_h = \{span(\phi_{i,j}(x,y)) \;\text{ such that }\; \phi_{i,j}(x,y) = 0, \;\text{ for }\; (x,y) \in \Gamma\}. \tag{22}$$

Taking into account (14) and (15) it is easy to check that [4]

$$\phi_{i,j}(x,y) = 0, \quad (x,y) \in \Gamma, \;\text{ for }\; i = 2,...,n-1, \; j = 2,...,m-1. \tag{23}$$

From (22) and (23) it follows that

$$\mathcal{V}_h = span\{\phi_{i,j}(x,y), \quad \text{for }\; i = 2,...,n-1, \; j = 2,...,m-1\}. \tag{24}$$

Hence, $u_0^h(x,y)$ can be written as

$$u_0^h(x,y) = \sum_{i=1}^{n} \sum_{j=1}^{m} \gamma_{i,j} \phi_{i,j}(x,y), \tag{25}$$

where $\gamma_{i,j} \in \mathbb{R}, \; i = 1,...,n, \; j = 1,...,m$. The coefficients $\gamma_{1,j}$, $\gamma_{n,j}$, for $j = 1,...,m$ and $\gamma_{i,1}, \gamma_{i,m}$, for $i = 1,...,n$ must be forced to be zero. In order to obtain a linear

system for the unknowns $\gamma_{i,j}$ it is convenient to vectorize the basis functions and the corresponding coefficients in (25) introducing the change of index

$$p := n(j-1)+i, \qquad i = 1, ..., n, \;\; j = 1, ..., m. \tag{26}$$

With this transformation, the expression (25) can be written as

$$u_0^h(x,y) = \sum_{p=1}^{N} \alpha_p \psi_p(x,y), \tag{27}$$

where $N := n \times m$ and

$$\begin{aligned} (\alpha_1, ..., \alpha_N)^t &= (\gamma_{1,1}, ..., \gamma_{n,1}, ..., \gamma_{1,m}, ..., \gamma_{n,m})^t, \\ (\psi_1(x,y), ..., \psi_N(x,y)) &= (\phi_{1,1}(x,y), ..., \phi_{n,1}(x,y), ..., \phi_{1,m}(x,y), ..., \phi_{n,m}(x,y)). \end{aligned} \tag{28}$$

The set of indexes $I = \{1, 2, ..., N\}$ is subdivided in two subsets: $I = I_0 \cup I_1$, where I_0 is the set of indexes of basis functions that generate $\mathcal{V}_h$ and I_1 is the set of indexes of basis functions that are different from 0 on Γ. In other words, $\mathcal{V}_h = span\{\psi_p(x,y),\ p \in I_0\}$ and I_1 is the set of indexes (26) corresponding to functions $\phi_{1,j}(x,y), \phi_{n,j}(x,y),\ j = 1, ..., m$ and $\phi_{i,1}(x,y), \phi_{i,m}(x,y),\ i = 1, ..., n$, hence $\alpha_p = 0$ for $p \in I_1$. Substituting in (10) expressions (20) and (21), changing $u(x,y)$ by $u_0^h(x,y)$ and $v(x,y)$ by the basis function $\psi_q(x,y),\ q \in I_0$, we obtain the Galerkin formulation: find $u_0^h(x,y)$ given by (27) such that

$$\begin{aligned} &\sum_{p \in I_0} \left[\int_0^1 \int_0^1 \left[(\nabla \psi_p)^t \, (J\mathbf{F}^t J\mathbf{F})^{-1} \nabla \psi_q - k^2 \psi_p \psi_q \right] |\det J\mathbf{F}| \, d\xi d\eta \right] \alpha_p \\ = \quad &\int_0^1 \int_0^1 \left[(f + k^2 u_g)\psi_q - (\nabla u_g)^t (J\mathbf{F}^t J\mathbf{F})^{-1} \nabla \psi_q \right] |\det J\mathbf{F}| \, d\xi d\eta, \;\; q \in I_0. \end{aligned}$$

In the last expression we omit the dependence of (ξ, η) of all functions in order to simplify the notation. These equations can be written in matrix form as

$$\mathbf{A}\widetilde{\boldsymbol{\alpha}} = \mathbf{b}, \tag{29}$$

where for $p,\ q \in I_0$

$$\mathbf{A} = (a_{q,p}) = \int_0^1 \int_0^1 \left[(\nabla \psi_p)^t \, (J\mathbf{F}^t J\mathbf{F})^{-1} \nabla \psi_q - k^2 \psi_p \psi_q \right] |\det J\mathbf{F}| \, d\xi d\eta, \tag{30}$$

and for $q \in I_0$

$$\mathbf{b} = (b_q) = \int_0^1 \int_0^1 \left[(f + k^2 u_g)\psi_q - (\nabla u_g)^t (J\mathbf{F}^t J\mathbf{F})^{-1} \nabla \psi_p \right] |\det J\mathbf{F}| \, d\xi d\eta, \tag{31}$$

and $\widetilde{\boldsymbol{\alpha}}$ is the vector of unknown coefficients $\alpha_p,\ p \in I_0$.

4. Computing the B-spline approximated solution.

In this section we explain how to compute a B-spline approximation of the function $u_g(x,y)$. Moreover, we give some details about the efficient implementation of the procedure to compute the global matrix and the right hand side vector of the linear system (29), whose solution is the vector $\boldsymbol{\alpha}$ of B-spline coefficients of $u_0^h(x,y)$.

4.1. Approximating the function $u_g(x,y)$. The function $u_g(x,y)$ satisfying boundary condition (5) is approximated by a function $u_g^h(x,y)$ in $\mathbb{S}_{3,t^\xi} \bigotimes \mathbb{S}_{3,t^\eta}$ written as

$$u_g^h(x,y) = \sum_{i=1}^{n}\sum_{j=1}^{m} \delta_{i,j}\phi_{i,j}(x,y), \tag{32}$$

with $\phi_{i,j}(x,y)$ given by (17). The unknown coefficients $\delta_{i,j},\ i=1,...,n,\ j=1,...,m$ are computed requiring that $u_g^h(x,y)$ interpolates the function $g(x,y)$, defining the Dirichlet boundary condition, at a sequence of points on Γ. More precisely, we select as interpolation sites $\widetilde{\xi}_i$ and $\widetilde{\eta}_j$ in the directions ξ and η respectively, the Greville abscissas, which for the quadratic interpolation are the averages of 2 consecutive knots in the sequences t^ξ and t^η

$$\widetilde{\xi}_k = \frac{t^\xi_{k+1}+t^\xi_{k+2}}{2}, \quad k=1,...,n, \tag{33}$$

$$\widetilde{\eta}_l = \frac{t^\eta_{l+1}+t^\eta_{l+2}}{2}, \quad l=1,...,m. \tag{34}$$

Evaluating the map $\mathbf{F}(\xi,\eta)$ given by (13) we obtain the sequence of interpolation points on Γ

$$\begin{aligned}(x_k^s,y_k^s) &:= \mathbf{F}(\widetilde{\xi}_k,0), \quad (x_k^n,y_k^n) := \mathbf{F}(\widetilde{\xi}_k,1), \quad k=1,...,n,\\ (x_l^w,y_l^w) &:= \mathbf{F}(0,\widetilde{\eta}_l), \quad (x_l^e,y_l^e) := \mathbf{F}(1,\widetilde{\eta}_l), \quad l=1,...,m.\end{aligned}$$

Recall that points $(x_k^s,y_k^s),(x_k^n,y_k^n),\ k=1,...,n$ are on the "south" and "north" boundaries of Ω, i.e in the boundary curves $\mathbf{F}(\xi,0)$ and $\mathbf{F}(\xi,1)$ respectively. Similarly, points $(x_l^w,y_l^w),(x_l^e,y_l^e)\ \ l=1,...,m$ are on the "west" and "east" boundaries of Ω, i.e in the boundary curves $\mathbf{F}(0,\eta)$ and $\mathbf{F}(1,\eta)$ respectively. In consequence, boundary coefficients of $u_g^h(x,y)$ in (32): $\delta_{i,1},\delta_{i,m},\ i=1,...,n$ and $\delta_{1,j},\delta_{n,j},\ j=1,...,m$, are computed from the interpolation conditions

$$\begin{aligned}u_g^h(x_k^s,y_k^s) = g(x_k^s,y_k^s), \quad u_g^h(x_k^n,y_k^n) = g(x_k^n,y_k^n), \quad k=1,...,n,\\ u_g^h(x_l^w,y_l^w) = g(x_l^w,y_l^w), \quad u_g^h(x_l^e,y_l^e) = g(x_l^e,y_l^e), \quad l=1,...,m.\end{aligned}$$

Taking into account that the boundary knots in the sequences (14) and (15) have multiplicity 3, from (32) and (17) we obtain that the previous interpolation conditions can be written as

$$\sum_{i=1}^{n}\delta_{i,1}B^3_{i,t^\xi}(\widetilde{\xi}_k) = g(x_k^s,y_k^s), \quad \sum_{i=1}^{n}\delta_{i,m}B^3_{i,t^\xi}(\widetilde{\xi}_k) = g(x_k^n,y_k^n), \quad k=1,...,n, \tag{35}$$

$$\sum_{j=1}^{m}\delta_{1,j}B^3_{j,t^\eta}(\widetilde{\eta}_l) = g(x_l^w,y_l^w), \quad \sum_{j=1}^{m}\delta_{n,j}B^3_{j,t^\eta}(\widetilde{\eta}_l) = g(x_l^e,y_l^e), \quad l=1,...,m. \tag{36}$$

Observe that linear systems (35) share the same matrix $B_1 := (B^3_{i,t^\xi}(\widetilde{\xi}_k))_{i,k=1}^n$ and linear systems (36) have the same matrix $B_2 := (B^3_{j,t^\eta}(\widetilde{\eta}_l))_{j,l=1}^m$. Matrices B_1 and B_2 are nonsingular since hypothesis of Shoenberg-Whitney theorem [4] hold for interpolation sites (33) and (34). Thus, coefficients $\delta_{i,1},\delta_{i,m},\ i=1,...,n$ and $\delta_{1,j},\delta_{n,j},\ j=1,...,m$ are computed solving the corresponding linear systems. The rest of the coefficients $\delta_{i,j},\ i=2,...,n-1,\ j=2,...,m-1$ are assigned as zero. Figure 2 shows the graphics of a region Ω and the corresponding function $u_g^h(x,y)$.

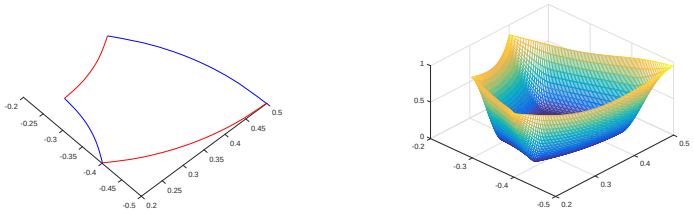

FIGURE 2. Left: physical domain Ω, right: function $u_g^h(x,y)$ satisfying Dirichlet boundary condition in Γ.

4.2. Assembling the global matrix and the right-hand side vector. The process of building the global matrix (30) and the vector (31) is known in the FEM literature as *assembly*. This process does not compute the elements of $\mathbf{A}$ and $\mathbf{b}$, one entry at a time, as a first glance at the formulation (30)-(31) might imply. Instead, one loops through the elements $\widehat{\Omega}_{k,l} := [\xi_k, \xi_{k+1}] \times [\eta_l, \eta_{l+1}]$, building as we go local matrices and vectors $\mathbf{A}^{k,l}$ and $\mathbf{b}^{k,l}$ respectively, for $k = 1, ..., n-2$, $l = 1, ..., m-2$. Every entry of each of these dense matrices and vectors is then added to the appropriate spot in the global matrix $\mathbf{A}$ and vector $\mathbf{b}$.

Since in our problem the basic functions are biquadratic B-splines, only 9 basic functions are different from zero in $\widehat{\Omega}_{k,l}$. These functions are

(37)
$$(\phi_{k,l},\ \phi_{k,l+1},\ \phi_{k,l+2},\ \phi_{k+1,l},\ \phi_{k+1,l+1},\ \phi_{k+1,l+2},\ \phi_{k+2,l},\ \phi_{k+2,l+1},\ \phi_{k+2,l+2}).$$

Therefore, each local matrix $\mathbf{A}^{k,l}$ and the corresponding vector $\mathbf{b}^{k,l}$ are of order 9×9 and 9×1 respectively. Denote by $p_1, ..., p_9$ the global indexes of basic functions (37) computed using (26). Then

$$\mathbf{A}^{k,l} = \begin{pmatrix} I_A(\psi_{p_1}, \psi_{p_1}) & \cdots & I_A(\psi_{p_1}, \psi_{p_9}) \\ I_A(\psi_{p_2}, \psi_{p_1}) & \cdots & I_A(\psi_{p_2}, \psi_{p_9}) \\ \vdots & \vdots & \vdots \\ I_A(\psi_{p_9}, \psi_{p_1}) & \cdots & I_A(\psi_{p_9}, \psi_{p_9}) \end{pmatrix} \tag{38}$$

where for $i, j = 1, ..., 9$

(39)
$$I_A(\psi_{p_i}, \psi_{p_j}) = \int_{\xi_k}^{\xi_{k+1}} \int_{\eta_l}^{\eta_{l+1}} \left[(\nabla \psi_{p_i})^t \, (J\mathbf{F}^t J\mathbf{F})^{-1} \nabla \psi_{p_j} - k^2 \psi_{p_i} \psi_{p_j} \right] |\det J\mathbf{F}| \, d\xi d\eta.$$

Similarly

$$\mathbf{b}^{k,l} = (I_b(\psi_{p_1}),\ I_b(\psi_{p_2}),\ \cdots, I_b(\psi_{p_9}))^t, \tag{40}$$

where for $i = 1, ..., 9$,

(41)
$$I_b(\psi_{p_i}) = \int_{\xi_k}^{\xi_{k+1}} \int_{\eta_l}^{\eta_{l+1}} \left[(f + k^2 u_g) \psi_{p_i} - (\nabla u_g)^t (J\mathbf{F}^t J\mathbf{F})^{-1} \nabla \psi_{p_i} \right] |\det J\mathbf{F}| \, d\xi d\eta.$$

The integrals (39) and (41) are computed approximately using Gaussian quadratures [22]. Observe that $I_A(\psi_{p_i}, \psi_{p_j})$, $i, j = 1, ..., 9$ must be added up in a_{p_i, p_j}. Similarly, $I_b(\psi_{p_i})$, $i = 1, ..., 9$ must be added up in b_{p_i}.

Finally, the approximated solution $u^h(x,y)$ of the problem is given by $u^h(x,y) = u_0^h(x,y) + u_g^h(x,y)$. From (32) and (25) it follows that

$$u^h(x,y) = \sum_{i=1}^{n}\sum_{j=1}^{m} \beta_{i,j}\phi_{i,j}(x,y), \tag{42}$$

where $\beta_{i,j} = \delta_{i,j} + \gamma_{i,j},\ i = 1,...,n,\ j = 1,...,m$.

Observe that equation (42) can be expressed also in terms of the tensor product B-spline basis (16) in the parametric space $\widehat{\Omega}$

$$u^h(\mathbf{F}(\xi,\eta)) \equiv u^h(\xi,\eta) = \sum_{i=1}^{n}\sum_{j=1}^{m} \beta_{i,j}B_{i,j}^3(\xi,\eta). \tag{43}$$

5. Numerical Experiments

In this section we describe our experiences solving the Helmholtz equation with Dirichlet boundary condition using IgA approach. Our study includes three model problems, where the exact solution is known and therefore, it is possible to compute the numerical errors. In the experiments we compute the L^2 *error* of the approximated solution $u^h(x,y)$ as

$$(L^2\ error)^2 \quad = \quad \int_0^1\int_0^1 \left(u(\mathbf{F}(\xi,\eta)) - u^h(\mathbf{F}(\xi,\eta))\right)^2\ |\det(J\mathbf{F}(\xi,\eta))\ |d\xi d\eta, \tag{44}$$

where $\mathbf{F}(\xi,\eta)$ was defined in (13) and $J\mathbf{F}(\xi,\eta))$ in (18). We also compute the H^1 *error* in the norm (8) as

$$\begin{aligned}(H^1\ error)^2 = (L^2\ error)^2 \quad &+ \quad \int_0^1\int_0^1 \left[\left(\frac{\partial u(\mathbf{F}(\xi,\eta))}{\partial x} - \frac{\partial u^h(\mathbf{F}(\xi,\eta))}{\partial x}\right)^2 + \ \cdots\right. \\ &+ \quad \left.\left(\frac{\partial u(\mathbf{F}(\xi,\eta))}{\partial y} - \frac{\partial u^h(\mathbf{F}(\xi,\eta))}{\partial y}\right)^2\right] |\det(J\mathbf{F}(\xi,\eta))|\ d\xi\ d\eta.\end{aligned} \tag{45}$$

In practice, we compute IgA errors with expressions (44) and (45) using a Gaussian quadrature rule in two variables with 4 points. The components of the (x,y) gradient $\nabla_{(x,y)}u^h = \left(\frac{\partial u^h}{\partial x}\ ,\ \frac{\partial u^h}{\partial y}\right)^t$ that appear in the expression (45) are calculated using the (ξ,η) gradient $\nabla_{(\xi,\eta)}u^h$, the Jacobian matrix (18) and the chain rule (19). The gradient $\nabla_{(\xi,\eta)}u^h$ is computed directly deriving in the expression (43) [1].

We consider several physical domains, with emphasis in planar regions Ω with irregular boundaries. The numerical results reported here have been obtained with the help of our computational implementation of isogeometric method. This implementation, uses biquadratic B-splines functions and computes the control points of the map $\mathbf{F}(\xi,\eta)$ that parametrizes Ω by minimizing a functional [1]. We run our experiments in a PC with i7 processor and 8Gb of RAM.

5.1. Poisson equation with discontinuous gradient. In this section we solve a very simple case of Helmholtz equation, the Poisson equation

$$-\Delta u(x,y) = f(x,y),\ \ (x,y) \in \Omega,$$

with Dirichlet boundary condition (2). The function $f(x,y)$ is computed in such a way that the exact solution $u(x,y)$ is given by

(46)
$$u(x,y) = \exp\left(\alpha\sqrt{(x-x_0)^2+(y-y_0)^2}\right) + \exp\left(\beta\sqrt{(x-x_1)^2+(y-y_1)^2}\right) + \exp\left(\gamma\sqrt{(x-x_2)^2+(y-y_2)^2}\right),$$

where the real values α, β and γ and the points (x_0,y_0), (x_1,y_1) and (x_2,y_2) are known. The function $g(x,y)$ is the restriction of $u(x,y)$ to the boundary of Ω. This problem is solved in [5] on the unit square $[0,1]^2$. Here we solve it on several irregular regions. The main difficulty is the discontinuity of the gradient of $u(x,y)$ in the points (x_0,y_0), (x_1,y_1) and (x_2,y_2).

In the following experiments $\alpha = \beta = \gamma = 7$ and the points involved in the description of the problem and in its solution (46) are: $(x_0,y_0) = \mathbf{F}(\xi_a,\eta_a)$, $(x_1,y_1) = \mathbf{F}(\xi_b,\eta_b)$ and $(x_2,y_2) = \mathbf{F}(\xi_c,\eta_c)$, where $\xi_a = \eta_a = 0.25$, $\xi_b = \eta_b = 0.5$ and $\xi_c = \eta_c = 0.75$. The first step to obtain the approximated solution u^h is to compute the B-spline biquadratic parametrization $\mathbf{F}(\xi,\eta)$ of the physical region Ω. The sequences of knots t^ξ and t^η that we use to define the space of biquadratic splines are *nonuniform*. More precisely, the distribution of knots in t^ξ is more concentrated near the parametric values ξ_a, ξ_b and ξ_c. Similarly, the sequence t^η contains more knots near the parametric values η_a, η_b and η_c.

In table 1 we show the results for different regions. The number of degrees of freedom $n \times m$ used to compute u^h is reported in the second column of the table. The other two columns contain the errors (44) and (45). As we observe, the L^2 error oscillates between e-01 and e-04, but the H^1 error is approximately one to two orders bigger. It means that u^h could be considered as acceptable approximation of the exact solution u, but partial derivatives of u^h are not good approximations of partial derivatives of u.

TABLE 1. Errors of the biquadratic B-spline solution of Poisson equation with exact solution (46) on several physical regions. The parameters ξ_a, ξ_b, ξ_c are simple knots in t^ξ and the parameters η_a, η_b, η_c are simple knots in t^η.

Region	Degrees of freedom	L^2 *error*	H^1 *error*
Havana bay	116×110	4.8168e-02	4.5843e-01
Toba lake	172×172	1.0143e-03	3.7642e-02
Strait of Gibraltar	96×112	6.2503e-01	1.1674e+00
Grijalva channel	124×44	1.0860e-02	4.2216e-01
Pátzcuaro lake	108×108	7.4703e-04	7.8701e-02
V. de Bravo reservoir	156×156	2.9897e-04	3.8636e-02

In Figure 3 we show the biquadratic B-spline functions u^h for some of the physical regions reported in table 1. We recall that the B-spline basis functions $B^3_{i,t^\xi}(\xi)$ and $B^3_{j,t^\eta}(\eta)$ used to construct the approximated solution u^h are C^1 continuous, since the corresponding sequences of knots t^ξ and t^η are composed by simple knots. However, the gradient of the exact solution (46) is not defined in three points. Hence, the smooth B-spline solution u^h approximates the exact solution u in these points, but partial derivatives of u^h are not good approximations of partial derivatives of u.

To overcome this difficulty, we include two times the parametric values ξ_a, ξ_b and ξ_c in the sequence of knots t^ξ, and similarly the parametric value η_a, η_b and η_c are included two times in the sequence t^η. The corresponding B-spline functions are only C^0 continuous in these points, therefore u^h approximates better the exact solution u. Observe that the introduction of new knots does not change the map $\mathbf{F}(\xi,\eta)$, which is still differentiable, but the expression of $\mathbf{F}(\xi,\eta)$ in the new basis must be computed.

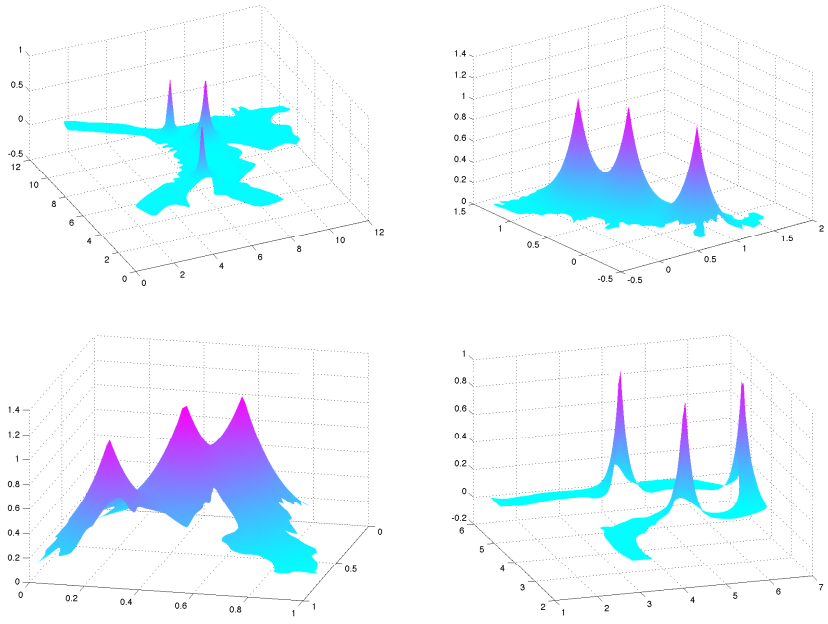

FIGURE 3. Biquadratic B-spline functions u^h approximating the exact solution (46) of Poisson equation for several regions. Top left: Havana bay, top right: Toba lake. Bottom left: V. de Bravo reservoir, bottom right: Grijalva channel.

In Figure 4 we compare the graph of the functions $u(\mathbf{F}(\xi,\xi))$ and $u^h(\mathbf{F}(\xi,\xi))$, where $\mathbf{F}$ is the parametrization of Pátzcuaro lake and u^h is the biquadratic B-spline approximation to the exact solution u. Observe that these curves contain the singular points of u. The left image shows the function $u(\mathbf{F}(\xi,\xi))$, $0 \le \xi \le 1$, while center and right images show a zoom of $u(\mathbf{F}(\xi,\xi))$ and $u^h(\mathbf{F}(\xi,\xi))$ restricted to the black rectangle in the left image. This rectangle contains the point $\xi_b = 0.5$. The center graph shows in blue the approximated B-spline solution u^h obtained for a sequence of simple knots. We observe that the exact solution $u(\mathbf{F}(\xi,\xi))$ (in red) is not differentiable in ξ_b, but $u^h(\mathbf{F}(\xi,\xi))$ has continuous derivative in this point. The right graph shows in blue the approximated B-spline solution u^h corresponding to a sequence of knots t^ξ, where $\xi_b = 0.5$ is repeated, and a sequence of knots t^η, where $\eta_b = 0.5$ is also repeated. The result is that u^h has the same behavior that u since it is not differentiable in $\xi_b = 0.5$. The effect of repeating the knots ξ_a, ξ_b and ξ_c in t^ξ and η_a, η_b and η_c in t^η is shown in table 2, which contains the results for the same physical regions of table 1.

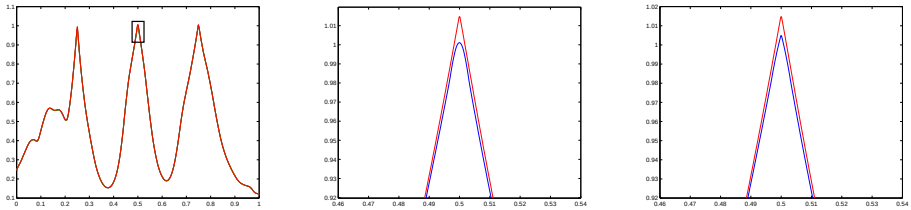

FIGURE 4. Left: graph of $u(\mathbf{F}(\xi,\xi))$ with u given by (46) on the Pátzcuaro lake. Center and right: zoom of $u^h(\mathbf{F}(\xi,\xi))$ (in blue) in comparison with $u(\mathbf{F}(\xi,\xi))$ (in red). In center graph u^h is computed with simple knots, in right graph u^h has repeated knots.

Comparing tables 1 and 2 we observe that in each parametric direction, the number of degrees of freedom is increased in 3, because we repeat 3 knots in the corresponding sequences t^ξ and t^η. As a consequence, the L^2 and the H^1 errors are reduced in general. The reduction is bigger for the H^1 error, since repeating knots we obtain a better approximation of the vector field of the exact solution. This is illustrated in Figure 5, where we show the vector field near a singular point for Havana bay. The left and center images of this figure show the vector field of the biquadratic B-spline function u^h for simple and repeated knots respectively. The right image shows the vector field of the exact solution u. It is easy to see that the size of the arrows near the singular point is smaller for the left image, which means that the field is smoother in this point. Moreover, the vector fields for the center and right images are very similar.

TABLE 2. Errors of the biquadratic B-spline solution of Poisson equation with exact solution (46). The parameters ξ_a, ξ_b, ξ_c are double knots in t^ξ and η_a, η_b, η_c are double knots in t^η.

Region	Degrees of freedom	L^2 *error*	H^1 *error*
Havana bay	119×113	4.7959e-02	3.4124e-01
Toba lake	175×175	1.0139e-03	2.6891e-02
Strait of Gibraltar	99×115	6.2427e-01	8.3259e-01
Grijalva channel	127×47	1.0598e-02	3.5410e-01
Pátzcuaro lake	111×111	7.4603e-04	7.3279e-02
V. de Bravo reservoir	159×159	2.9866e-04	3.5940e-02

5.2. Helmholtz equation with constant wave number. In this section we solve the Helmholtz equation (1), where the function $k(x,y)$ is a constant $k > 0$, and the right hand side is

$$f(x,y) = \left(\frac{5\pi^2 - 4}{4}\right) k^2 \, sin(k\pi x)\, sin(k\pi y/2).$$

This equation has exact solution

$$u(x,y) = sin(k\pi\, x)\, sin(k\pi y/2). \tag{47}$$

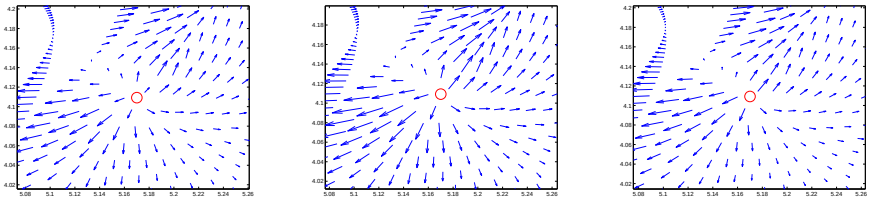

FIGURE 5. Zoom of the vector field of the exact solution and the biquadratic B-spline solution of Poisson equation. Left: for the smooth B-spline approximation with simple knots. Center: for the B-spline approximation with double knots. Right: for the exact solution.

The function (47) is very oscillatory and the number of its oscillations is higher as k grows. Moreover, the function

$$\|\nabla u\|^2 = \left(\frac{\partial u}{\partial x}\right)^2 + \left(\frac{\partial u}{\partial y}\right)^2, \tag{48}$$

is even more oscillatory than $u(x, y)$, as we can see in Figure 6, where functions (47) and (48) are shown for $k = 1$ on $[0, 2\pi] \times [0, 4\pi]$. We will see soon, that this behavior of $\|\nabla u\|^2$ makes difficult to obtain good approximations of $u(x, y)$ in the H^1 norm.

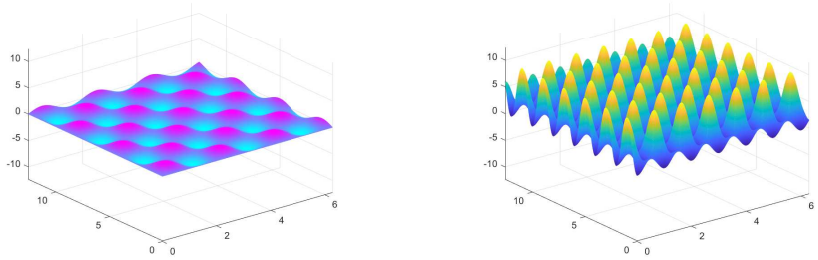

FIGURE 6. Function $u(x, y)$ given by (47) on $[0, 2\pi] \times [0, 4\pi]$ for $k = 1$ (left) and the corresponding function $\|\nabla u\|^2$ given by (48) (right).

5.2.1. Influence of the wave number k in the error. Here we solve the Helmholtz equation (1) in a region Ω, that is a closed approximation of Havana bay (see Figure 1). The first step to solve the problem is to parametrize Ω with an injective biquadratic map $\mathbf{F}(\xi, \eta)$. In this example, we use a *uniform* sequence of knots in both directions ξ and η. The $n \times m$ control points of $\mathbf{F}(\xi, \eta)$ in (13) are computed as the vertices of a quadrilateral mesh [1]. In Figure 1 we show the control mesh for $n = 38$ and $m = 38$. First, we solve the problem for $k = 1$. The corresponding solution u^h, written as (42), belongs to the space of biquadratic B-splines functions, with uniform knots and $N = n \times m = 1\,444$ degrees of freedom. The errors (44) and (45) in the L^2 and H^1 norms are 2.7801e-05 and 5.3929e-03

respectively. Since the number of oscillations of u grows when we increase the parameter k, more degrees of freedom are necessary, if we want to obtain similar errors in the L^2 and H^1 norms.

TABLE 3. Errors, for different values of k, of the biquadratic B-spline solution of Helmholtz equation with exact solution (47) on Havana bay domain.

k	n_{sub}	Degrees of freedom	L^2 *error*	H^1 *error*
1	1	38×38	2.7801e-05	5.3929e-03
3	2	74×74	3.9801e-05	1.4816e-02
5	3	146×146	1.4232e-05	1.1136e-02
10	4	290×290	9.0835e-06	1.6026e-02
15	5	578×578	3.3467e-06	1.1990e-02

To increase the number of degrees of freedom, we insert new knots located at the midpoints between old knots. The control points of the (same) map $\mathbf{F}(\xi, \eta)$ are updated using subdivision. The extra degrees of freedom obtained allow to keep the errors bounded. In table 3 we show the errors (44) and (45), obtained solving the problem with $k = 1, 3, 5, 10, 15$. The second column of the table indicates the number n_{sub} of subdivisions of the original control mesh (with $n \times m$ control points, $n = 38$ and $m = 38$) that we made, in order to increase the total number of degrees of freedom reported in the third column. Two things are clear: the H^1 error is at about two orders bigger than the L^2 error. Moreover, to keep the L^2 error between e-05 and e-06 and the H^1 error between e-02 and e-03, more degrees of freedom are necessary as we increase the value of k.

In Figure 7 we show the approximated solution u^h for $k = 15$, obtained with $n = 578$ and $m = 578$ for a total of $N = 334\,084$ degrees of freedom. The L^2 and H^1 errors, reported in table 3 are of order e-06 and e-02 respectively.

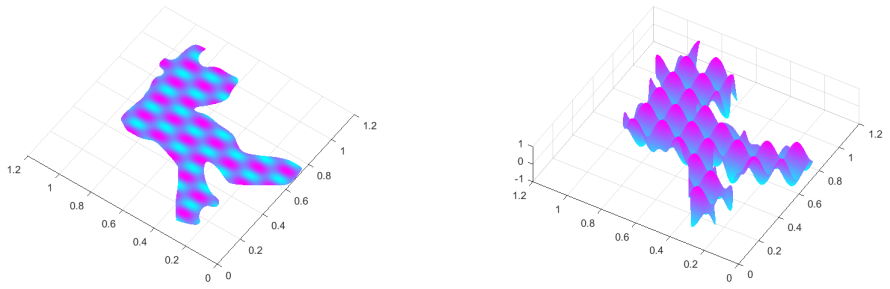

FIGURE 7. Approximated solution u^h of Helmholtz equation with exact solution (47) for $k = 15$. Function u^h is computed using biquadratic B-splines with $578 \times 578 = 334\,084$ degrees of freedom. Left: 2D view, right: 3D view.

5.2.2. Influence of the parametrization in the error. It is well known that the precision of the approximated solution computed with IgA approach depends on the quality of the parametrization $\mathbf{F}(\xi,\eta)$ of the physical domain Ω [26]. In this sense, a good *uniformity* and *orthogonality* of the isoparametric curves of $\mathbf{F}(\xi,\eta)$ is desirable. To measure the quality of the parametrization in the point $\mathbf{F}(\xi,\eta)$ we use the *mean ratio Jacobian* [25] given by

$$J_r(\xi,\eta) = \frac{2\det J\mathbf{F}(\xi,\eta)}{\|\mathbf{F}_\xi(\xi,\eta)\|_2^2 + \|\mathbf{F}_\eta(\xi,\eta)\|_2^2}, \tag{49}$$

where $\mathbf{F}_\xi(\xi,\eta) = (\frac{\partial x}{\partial \xi}, \frac{\partial y}{\partial \xi})$ and $\mathbf{F}_\eta(\xi,\eta) = (\frac{\partial x}{\partial \eta}, \frac{\partial y}{\partial \eta})$ are the tangent vectors to the isoparametric curves, and $\|\cdot\|_2$ denotes the Euclidean norm. If the map $\mathbf{F}(\xi,\eta)$ is injective, then $\det J\mathbf{F}(\xi,\eta)$ does not changes of sign. Assuming that $\det J\mathbf{F}(\xi,\eta) > 0$ it holds that $0 < J_r(\xi,\eta) \leq 1$. A value of J_r equal to 1 at a point $\mathbf{P}_0 = \mathbf{F}(\xi_0,\eta_0)$ indicates that the isoparametric curves are orthogonal at $\mathbf{P}_0$ and the map $\mathbf{F}(\xi,\eta)$ produces the same length distortion at $\mathbf{P}_0$ in both parametric directions ξ and η. On the contrary, a value of J_r close to zero indicates a poor parametrization.

To study the influence of the parametrization in the accuracy of the numerical results we solve Helmholtz equation with exact solution (47) for three different regions: Blue lagoon, Ucha lake and Jyvasjarvi lake. For each region a parametrization $\mathbf{F}(\xi,\eta)$ of the domain Ω is computed. In first row of Figure 8 we show a color map, where colors correspond to the values of $J_r(\xi,\eta)$ for the parametrization $\mathbf{F}(\xi,\eta)$. Yellow areas in Ω have a value of J_r close to 1, while blue areas are those where J_r is close to 0. In other words, in blue zones the parametrization is poor.

Moreover, we construct a rectangular mesh of points $(\widetilde{\xi}_i, \widetilde{\eta}_j)$, $i = 1, ..., \widetilde{n}$, and $j = 1, ..., \widetilde{m}$ in $[0,1] \times [0,1]$. Given the parametrization $\mathbf{F}(\xi,\eta)$ of the region Ω, let $(\widetilde{x}_i, \widetilde{y}_j) = \mathbf{F}(\widetilde{\xi}_i, \widetilde{\eta}_j)$ be the vertices of the corresponding rectangular mesh in Ω. To show the influence of the parametrization $\mathbf{F}(\xi,\eta)$ in the accuracy of IgA approximated solution, we compute for each point $(\widetilde{\xi}_i, \widetilde{\eta}_j)$ the *pointwise* H^1 *error*, denoted by eH_p^1 and defined as

$$(eH_p^1)^2\Big|_{(\widetilde{x}_i,\widetilde{y}_j)} = (u-u^h)^2\Big|_{(\widetilde{x}_i,\widetilde{y}_j)} + \left(\frac{\partial u}{\partial x} - \frac{\partial u^h}{\partial x}\right)^2\Big|_{(\widetilde{x}_i,\widetilde{y}_j)} + \left(\frac{\partial u}{\partial y} - \frac{\partial u^h}{\partial y}\right)^2\Big|_{(\widetilde{x}_i,\widetilde{y}_j)}.$$

In the second row of Figure 8 we plot on the mean ratio Jacobian map a red point in the coordinates $(\widetilde{x}_i, \widetilde{y}_j)$, if $eH_p^1(\widetilde{x}_i, \widetilde{y}_j)$ is greater than a given threshold ε. The value of ε is selected for each region, depending of the range of values of the pointwise H^1 error. For Blue lagoon we solve Helmholtz equation with $k = 3$ and compute IgA solution with $n \times m$ degrees of freedom with $n = m = 234$. Helmholtz equation with $k = 10$ was solved on Ucha lake, with $n = m = 134$. Finally, on Jyvasjarvi lake we solve Helmholtz equation with $k = 5$ and compute IgA solution using $n \times m$ degrees of freedom with $n = m = 74$.

From Figure 8 it is clear that most of points with high *pointwise* H^1 *error* are located in those zones where the parametrization of Ω is poor (intense blue areas in the mean ratio Jacobian map). It confirms that the precision of the approximated solution computed with IgA approach depends on the quality of the parametrization of the physical domain, with smaller errors in zones of Ω with high quality parametrization. This is very significant in some applications, where due to the physical nature of the problem, it is important to have small error in some specific areas of the domain.

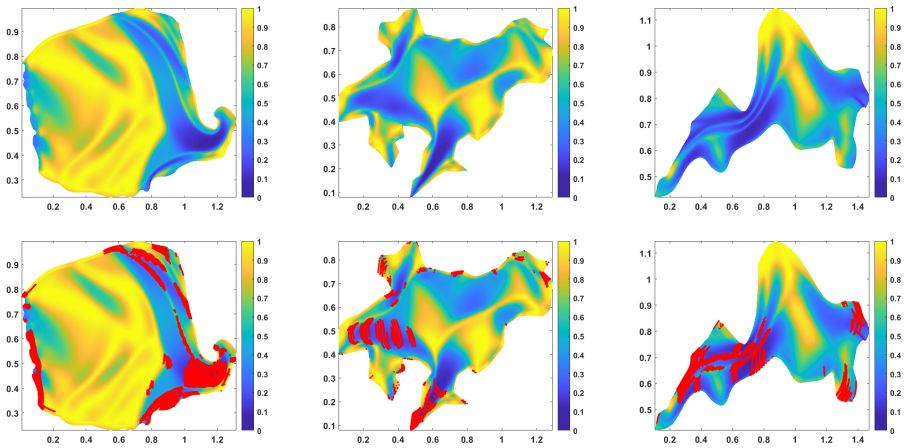

FIGURE 8. First row: mean ratio Jacobian map, dark blue areas are zones of poor parametrization. Second row: red points on mean ratio Jacobian map are those where the *pointwise* H^1 error is bigger than a prescribed threshold. Left: Blue lagoon region, center: Ucha lake, right: Jyvasjarvi lake.

5.2.3. Comparison with FEM solution. Given a physical domain Ω, in this section we compute a sequence of IgA approximated solutions of Helmholtz equation with exact solution (47). Moreover a sequence of quadratic FEM solutions is also computed and a comparison between them is performed. To obtain these sequences of solutions we proceed as follows. First, we construct a biquadratic B-spline parametrization $\mathbf{F}(\xi,\eta)$ of Ω written as (13) and with uniform knots t^{ξ} and t^{η}.

The sequence of IgA solutions is computed increasing the number of degrees of freedom by knot insertion. Starting from the original knots (14) and (15), that we denote here by $t^{\xi,0}$ and $t^{\eta,0}$, the new sequences of knots $t^{\xi,1}$ and $t^{\eta,1}$ are obtained inserting new knots at the midpoints of the break points. More precisely, $t^{\xi,1} = (0,0,\xi_1^1,\xi_2^1,...,\xi_{2n-3}^1,1,1)$, where $\xi_{2i-1}^1 = \xi_i$ for $i = 1,...,n-1$ and $\xi_{2i}^1 = (\xi_i+\xi_{i+1})/2$, for $i = 1,...,n-2$. The sequence $t^{\eta,1} = (0,0,\eta_1^1,\eta_2^1,...,\eta_{2m-3}^1,1,1)$ is constructed in a similar way. Repeating the previous strategy we obtain sequences of knots $t^{\xi,l}$ and $t^{\eta,l}$ for $l > 1$. These knots define a sequence of nested tensor product *biquadratic spline spaces* $\mathbb{S}_{3,t^{\xi,l}} \bigotimes \mathbb{S}_{3,t^{\eta,l}}$. IgA approximated solutions computed here belong to these spaces.

FEM approximated solution is computed for a sequence of meshes $\mathcal{M}^l$ defined as follows. Vertices $\mathcal{M}_{i,j}^l$ of the mesh $\mathcal{M}^l$ with $l \geq 0$ are computed as $\mathcal{M}_{i,j}^l = \mathbf{F}(\xi_i^l,\eta_j^l)$, where ξ_i^l and η_j^l are the break points defining the knot sequences $t^{\xi,l}$ and $t^{\eta,l}$ respectively. For each mesh of the sequence $\mathcal{M}^l$, $l = 0,1...$, we solve the Helmholtz equation using FEM *quadratic Lagrange elements with 9 nodes*. If we denote by h the mesh size of $\mathcal{M}^0$, the number N_{FEM} of degrees of freedom of FEM solution on $\mathcal{M}^0$ is proportional to $4/h^2$. In comparison, the number N_{IgA} of degrees of freedom of IgA solution in $\mathbb{S}_{3,t^{\xi,0}} \bigotimes \mathbb{S}_{3,t^{\eta,0}}$ is proportional to $1/h^2$, with h denoting as before the mesh size of $\mathcal{M}^0$. Since $\mathbf{F}(\xi,\eta)$ is biquadratic, then the mesh size of $\mathcal{M}^1$ is approximately $h/2$. From the previous analysis we conclude that

refining the mesh $\mathcal{M}^0$, the mesh size is reduced from h to $h/2$, the number N_{FEM} of degrees of freedom of FEM solution is increased from $4/h^2$ to $16/h^2$, while the number N_{IgA} of degrees of freedom of IgA solution is increased from $1/h^2$ to $4/h^2$. In other words, the value of N_{FEM} for the mesh $\mathcal{M}^0$ of size h is of the same order that the value of N_{IgA} for the mesh $\mathcal{M}^1$ of size $h/2$.

In [2], some results about a priori error estimate of IgA solutions under quasi uniform h-refinement are presented. For second order elliptic PDE, with exact solution $u \in H^{p+1}(\Omega)$, where p is the minimum of polynomial degrees in directions ξ and η, it is shown that the L^2 error of IgA solution u^h is bounded by

$$||u - u^h||_{L^2(\Omega)} \leq C\, h^{p+1} ||u||_{H^{p+1}(\Omega)}. \tag{50}$$

Moreover, the H^1 error is bounded by

$$||u - u^h||_{H^1(\Omega)} \leq C\, h^{p} ||u||_{H^{p+1}(\Omega)}. \tag{51}$$

Hence, the *order of convergence* of IgA and classical FEM are the same for degree p basis functions. Since in $2D$ problems the number of degrees of freedom (dof) is of order h^{-2}, from (50) and (51), the order of convergence is $(dof)^{-(p+1)/2}$ in the L^2 norm and $(dof)^{-p/2}$ in H^1 norm. In particular, for $p = 2$, the expected order of convergence of L^2 and H^1 errors are $(dof)^{-3/2}$ and $(dof)^{-1}$ respectively, for both FEM and IgA approximations.

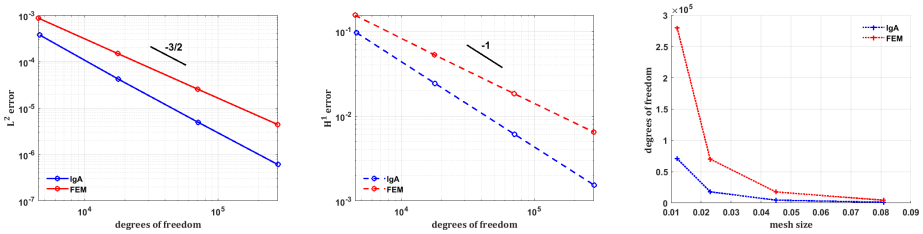

FIGURE 9. Ucha lake results for $k = 5$. L^2 error (left) and H^1 error (center), both *log-log* plots as functions of the number of degrees of freedom (dof). Right: number of dof vs. mesh size h. Blue: IgA solution, red: FEM solution.

In the next experiments we show that, even when the errors of IgA and FEM are of the same order, the computational cost of FEM is higher, since it requires approximately 4 times more dof than IgA to obtain these errors. This increment in the number of dof of FEM is more significant for higher values of p. Quoting Cottrell et al in [8] *" the isogeometric analysis solution obtained using NURBS of order p has the same order of convergence as we would expect in a classical FEA setting using classical basis functions with a polynomial order of p ... bisecting all of the elements in an FEA mesh (thus cutting the mesh parameter from h to h/2) requires the introduction of many more degrees of freedom than does bisection of the same number of NURBS elements while maintaining p − 1 continuity. This means that NURBS can converge at the same rate as FEA polynomials, while remaining much more efficient".*

To evaluate the results obtained with FEM and IgA, we solve the Helmholtz equation with exact solution (47) for different regions. In Figures 9, 10 and 11 we show the results for three regions: Ucha lake, Banderas bay and Titicaca lake. The

log of L^2 error (left) and the *log* of H^1 error (center) are plotted, for FEM and IgA approximated solutions, both as functions of *log* of the number of degrees of freedom. Observe that in all examples the L^2 error is of order $(dof)^{-3/2}$, while the H^1 error is of order $(dof)^{-1}$ for both FEM and IgA. Nevertheless, it is clear that for a given number of degrees of freedom, IgA solution is about half an order of magnitude more accurate than FEM solution. Moreover, this behavior is more pronounced when we increase the number of degrees of freedom. The right column in Figures 9, 10 and 11 show a graph of the number of degrees of freedom of FEM and IgA, N_{FEM} and N_{IgA} respectively, as function of the mesh size h. Notice that the value of N_{FEM} for the mesh $\mathcal{M}^l$ of size h is similar to the value of N_{IgA} for the mesh $\mathcal{M}^{l+1}$ of size $h/2$. Since the errors of IgA and FEM solutions are of the same order (as functions of h), this confirm that given a mesh size h, FEM solution requires more dof than IgA solution to obtain L^2 and H^1 errors of the same order. This implies that the computational cost of FEM is higher, since at least dof^2 operations are need to solve a linear system with dof unknowns.

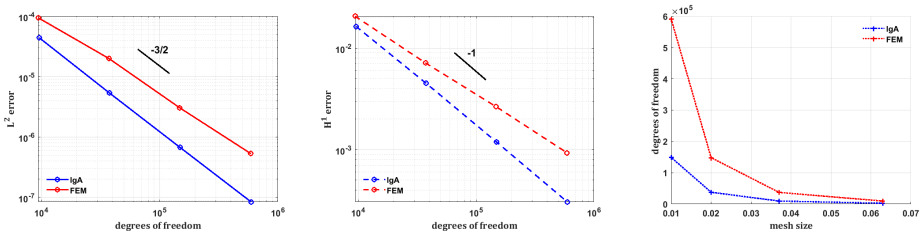

FIGURE 10. Banderas bay results for $k = 3$. L^2 error (left) and H^1 error (center), both *log-log* plots as functions of the number of degrees of freedom (dof). Right: number of dof vs. mesh size h. Blue: IgA solution, red: FEM solution.

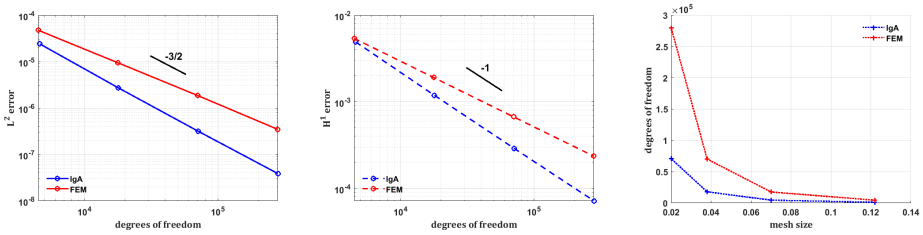

FIGURE 11. Titicaca lake results for $k = 1$. L^2 error (left) and H^1 error (center), both *log-log* plots as functions of the number of degrees of freedom (dof). Right: number of dof vs. mesh size h. Blue: IgA solution, red: FEM solution.

Experiments with other regions with irregular boundary and higher values of k confirm the results reported in Figures 9, 10 and 11. As an example we show in table 4 the L^2 errors of FEM and IgA approximated solutions, both computed for the sequence of mesh refinements explained before, for three regions: Valle Bravo reservoir (with $k = 25$), Aral sea (with $k = 20$) and Gibraltrar strait (with $k = 15$).

TABLE 4. L^2 errors of FEM and IgA approximated solutions for a sequence of mesh refinements and three irregular regions.

Region	Valle Bravo ($k=25$)		Aral ($k=20$)		Gibraltar ($k=15$)	
	dof	L^2 error	dof	L^2 error	dof	L^2 error
IgA	4624	1.2904e-01	6384	7.3934e-02	10764	3.0033e-03
FEM	4489	7.1431e-01	6179	5.9143e-02	10549	6.2688e-03
IgA	17956	6.6323e-03	24716	9.9665e-03	42196	2.9474e-04
FEM	17689	6.4833e-02	24309	1.1141e-02	41769	1.0030e-03
IgA	70756	4.9397e-04	97236	6.8826e-04	167076	3.3809e-05
FEM	70225	6.0208e-03	96425	2.1565e-03	166225	1.5478e-04
IgA	280900	5.3282e-05	385700	6.8921e-05	664900	4.1310e-06
FEM	279841	7.8168e-04	384081	2.5806e-04	663201	2.4403e-05

Like in the previous examples we observe that, for similar numbers of degrees of freedom, IgA solution is at least half an order of magnitude more accurate than FEM solution in the L^2 norm. This behavior is again more accentuated when the number of degrees of freedom is increased.

5.3. Helmholtz equation with variable wave number. The wave function $u(x,y)$ that satisfies a Schrödinger equation model of two interacting atoms [28] is the solution of the Helmholtz equation (1) with

$$k(x,y) = \frac{1}{\alpha + r(x,y)}, \tag{52}$$

where α is a parameter, $r(x,y) = \sqrt{(x-x_0)^2 + (y-y_0)^2}$ and

$$f(x,y) = \frac{(\alpha - r(x,y))\cos(k(x,y))}{(\alpha + r(x,y))^3 r(x,y)}. \tag{53}$$

In this case, the exact solution of Helmholtz equation is given by

$$u(x,y) = \sin(k(x,y)). \tag{54}$$

The function (54) has discontinuous gradient at (x_0, y_0) and it is highly oscillatory near that point. The number of oscillations M is determined by the parameter $\alpha = \frac{1}{M\pi}$.

5.3.1. Experiments when the exact solution has only one oscillation. In this section we solve the Helmholtz equation with $k(x,y)$ given by (52) for several regions with irregular boundary. In all the examples we select $\alpha = \frac{1}{\pi}$ and we compute the point (x_0, y_0) as $\mathbf{F}(\widetilde{\xi}, \widetilde{\eta})$, where $(\widetilde{\xi}, \widetilde{\eta}) = (0.5, 0.5)$ and the parametrization $\mathbf{F}(\xi, \eta)$ is the biquadratic B-spline function given by (13), with control points computed as the vertices of a quadrilateral mesh [1].

Initially the sequences of knots t^ξ and t^η are defined by (14) and (15) respectively. But new knots are inserted depending on the position of the point $(\widetilde{\xi}, \widetilde{\eta})$. More precisely, if $t_i^\xi < \widetilde{\xi} < t_{i+1}^\xi$ then the knot sequence (14) is refined inserting 9 equally spaced knots in each interval $(t_{i-1}^\xi, t_i^\xi), (t_i^\xi, t_{i+1}^\xi)$ and $(t_{i+1}^\xi, t_{i+2}^\xi)$. Similarly, if $t_j^\eta < \widetilde{\eta} < t_{j+1}^\eta$ then we insert in (15) 9 knots equally spaced in each interval $(t_{j-1}^\eta, t_j^\eta), (t_j^\eta, t_{j+1}^\eta)$ and $(t_{j+1}^\eta, t_{j+2}^\eta)$. If $\widetilde{\xi}$ or $\widetilde{\eta}$ agrees with a knot of the sequences t^ξ and t^η respectively, then we insert 9 equally spaced knots in both intervals of t^ξ and

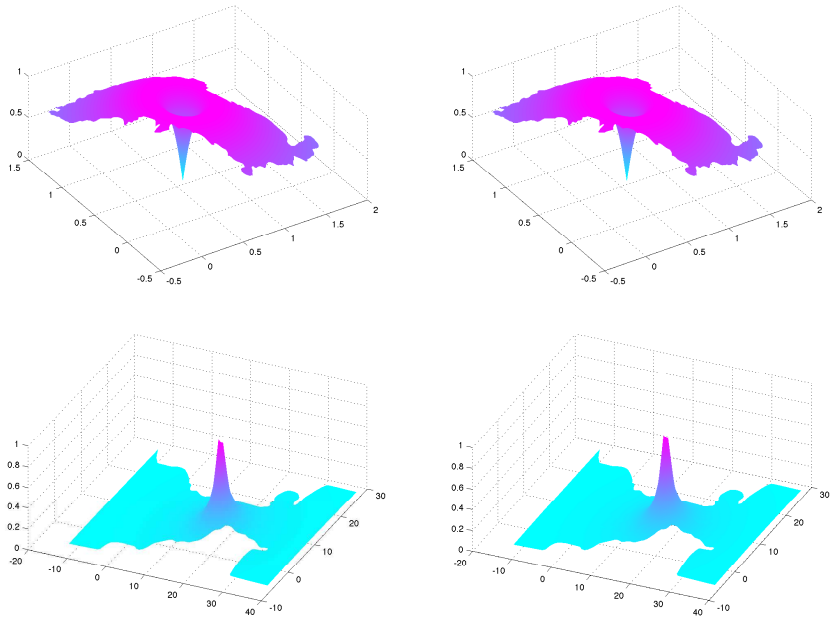

FIGURE 12. Biquadratic B-spline solution u^h and exact solution (54) of Helmholtz equation with variable wave number. Left column: B-spline approximation u^h. Right column: exact solution (54). First row Toba lake, second row Strait of Gibraltar.

t^η containing the value $\widetilde{\xi}$ and $\widetilde{\eta}$. Finally, since the gradient of the exact solution u is discontinuous in (x_0, y_0) we always insert $\widetilde{\xi} = \widetilde{\eta} = 0.5$ as a double knot in t^ξ and also as a double knot in t^η.

TABLE 5. Errors of the biquadratic B-spline solution of Helmholtz equation with exact solution (54) on several physical regions.

Region	Degrees of freedom	L^2 *error*	H^1 *error*
Havana bay	117×111	2.1853e-02	7.9875e-02
Toba lake	167×167	1.6721e-03	2.0115e-02
Strait of Gibraltar	97×157	1.5081e-01	2.5876e-01
Grijalva channel	119×39	3.0655e-03	8.7938e-02
Pátzcuaro lake	109×109	7.6203e-04	8.7178e-02
V. de Bravo reservoir	157×157	2.1475e-04	1.3584e-02

Figure 12 shows the graph of the exact solution u and the approximated biquadratic B-spline solution u^h for two of the regions reported in table 5. For each row, the graph in left column is u^h and the graph in the right column is u. The differences between u and u^h are not appreciable. In table 5 we show the errors of the biquadratic B-spline solution u^h for different physical regions. The L^2 error oscillates between e-01 and e-04. The H^1 error is in some cases of the same order as L^2, but it can grow up to two orders in others.

5.3.2. Experiments increasing the number of oscillations of the exact solution. As we already mentioned, the parameter M in the expression of $\alpha = \frac{1}{M\pi}$ is the number of oscillations of the exact solution (54). Hence, in order to obtain a good approximation u^h of the exact solution u, for values of M greater than 1 we must add more basic functions $B_i^3(\xi)$ and $B_j^3(\eta)$ different from zero near $\widetilde{\xi} = \widetilde{\eta} = 0.5$. In our experiments, we always insert $\widetilde{\xi} = \widetilde{\eta} = 0.5$ as a double knot in t^ξ and also as a double knot in t^η. Moreover, a total of 27 equally spaced knots are inserted in both intervals in t^ξ containing $\widetilde{\xi}$. The same procedure is used for inserting knots in t^η.

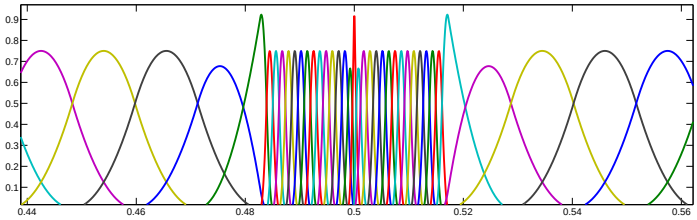

FIGURE 13. Some basis functions $B^3_{i,t^\xi}(\xi)$ after insertion of knots near $\xi = 0.5$.

In Figure 13 we show some of the basis functions $B^3_{i,t^\xi}(\xi)$, $0 \le \xi \le 1$. Since the knots are very concentrated in the neighborhood of $\widetilde{\xi} = 0.5$, we observe that many basic functions (one for each knot inserted) are different from 0 near this value.

In the next examples we solve the Helmholtz equation with exact solution (54) for $M = 2$, $M = 3$ and $M = 4$. In table 6 we show the L^2 and the H^1 errors of the approximated solution u^h, when the physical domain is Havana bay. For comparison, we also include the result of table 5 for $M = 1$. Observe that the number of degrees of freedom, reported in column 2, is bigger for $M > 1$ than for $M = 1$.

Figure 14 shows the graph of the functions $u(\mathbf{F}(\xi,\eta))$ and $u^h(\mathbf{F}(\xi,\eta))$ for Havana bay, both restricted to the parametric line $\xi = \eta$, which contains the pre-image of the singular point (x_0, y_0). More precisely, the red graph shows the curve $u(\mathbf{F}(\xi,\xi))$, while the blue graph represents the function $u^h(\mathbf{F}(\xi,\xi))$. The first row corresponds to the solution with $M = 2$ oscillations, the second and third rows correspond to $M = 3$ and $M = 4$ respectively. In each row, the black rectangle area in the graph is zoomed in the next right image. Observe that the oscillations are located is a very narrow segment. Moreover, the approximated solution u^h reproduces the behavior of u including the non differentiability in the point $\widetilde{\xi} = 0.5$. Finally, we point out that even when the region Ω is irregular and the number of oscillations of the exact solution is increased, the L^2 and H^1 errors remain bounded.

5.3.3. Convergence study. To study the convergence of the isogeometric approach we solve in this section the Helmholtz equation, where $k(x,y)$ and $f(x,y)$ are given by (52) and (53) respectively, Ω is the Jigsaw puzzle region given in [20] and shown in Figure 15, and $\alpha = \frac{1}{\pi}$. In table 7 we report the L^2 and the H^1 errors for increasing values of the number $N = n \times m$ of degrees of freedom. The i-th row of table 7 corresponds to a sequence of knots which is obtained refining uniformly

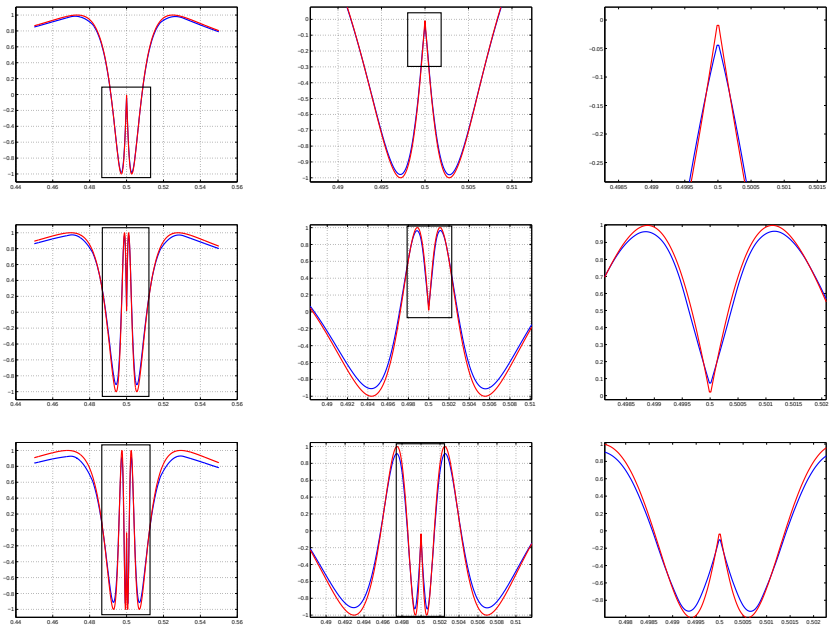

FIGURE 14. Restriction to a parametric line of the exact (red) and approximated (blue) solutions of the Helmholtz equation with variable wave number on Havana bay. Each rectangle area is amplified on right image in the same row. First row $M = 2$, second row $M = 3$ and third row $M = 4$.

TABLE 6. Errors on Havana bay of the biquadratic B-spline solution of Helmholtz equation, with exact solution (54) for increasing number M of oscillations.

Number of oscillations (M)	Degrees of freedom	L^2 *error*	H^1 *error*
1	117×111	2.1853e-02	7.9875e-02
2	171×165	3.3136e-02	1.6737e-01
3	171×165	7.9149e-02	4.8330e-01
4	171×165	1.4820e-01	8.4187e-01

$i-1$ times the initial uniform sequences (14) and (15) and introducing later equally spaced knots in the intervals containing the parametric value 0.5 in each direction (see the previous section). As we observe the L^2 and the H^1 errors decrease as the number of degrees of freedom increases.

In Figure 15 we show a 2D view of the approximated solution for three of the cases reported in table 7. There are almost no differences between the approximated solution with $537 \times 537 = 288\,369$ degrees of freedom and the exact solution.

6. Conclusions

The solution of partial differential equations with IgA approach has several advantages in comparison with the classical finite element method. One of them is

TABLE 7. Errors on Jigsaw puzzle region of the biquadratic B-spline solution of Helmholtz equation, with exact solution (54) for increasing number of degrees of freedom.

Degrees of freedom	L^2 *error*	H^1 *error*
13×13	1.9015e+00	2.8427e+00
25×25	5.2472e-01	1.0000e+00
45×45	1.5823e-01	3.8434e-01
81×81	5.7594e-02	1.5188e-01
149×149	2.2850e-02	6.9488e-02
281×281	9.5391e-03	3.4967e-02
537×537	4.7848e-03	1.8761e-02

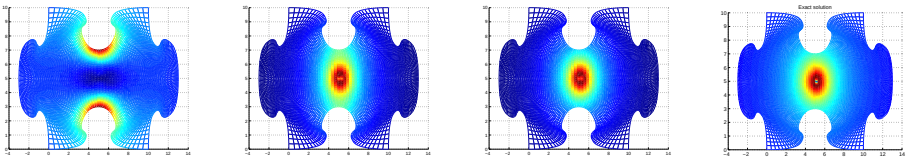

FIGURE 15. 2D views of the approximated IgA solution of the Helmholtz equation when we increase the number of degrees of freedom. From left to right the total number N of dof is: 169, 625 and 288 369. Right image corresponds to the exact solution (54).

that the boundary of the physical domain is represented exactly. This is specially important when the boundary is irregular, since high errors may be introduced if it is approximated. In this paper we have confirmed that, in the context of the numerical solution of the Helmholtz equation with Dirichlet boundary condition.

In contrast with previous works that deal with closed domains with very simple boundary curves, we have solved Helmholtz equation on regions with very irregular boundary. For these regions, the first step of IgA approach: the construction of a good parametrization of the domain, is qualitatively more complex. Moreover, we have considered Dirichlet boundary condition, the more challenging for the convergence of iterative Krylov-type solvers, usually employed for the numerical solution of the linear system derived from the discretization.

In our implementation of IgA, biquadratic B-spline functions are used to compute a parametrization of the physical domain and also as a basis for writing the approximated solution of the Helmholtz equation. The success of the method is proved solving several difficult model problems, for which the exact solution has singular points or is highly oscillatory. A lot of experiments have been included, both for constant a variable wave number. Special attention is paid to the selection of the number and position of the knots of the B-splines functions, in such a way that the approximated solution reproduces the behavior of the exact solution. In this sense, IgA approach is also advantageous, since it is able to offer smooth solutions having at the same time some singular points and high number of oscillations. The influence of the wave number and the quality of the parametrization of the physical domain in the accuracy of the numerical solution was also studied. IgA

and FEM quadratic approximated solutions are compared through several examples, which confirm that even when the L^2 and H^1 errors are of the same order, the computational cost of FEM is higher, since it requires more degrees of freedom than IgA to obtain these errors. In other words, in comparison with FEM, IgA provides improved accuracy per degree of freedom.

As a future work we plan to solve the Helmholtz equation using IgA approach, when the wave number is large. This problem, very important in acoustics and other applications, is difficult to solve with classical FEM. Our intention is to show that IgA approach is a better option to obtain good approximated solutions. Moreover, we want to explore deeper the relation between the local quality of the parametrization of the physical domain and the local error of IgA solution.

Acknowledgements

We are very grateful to colleagues of UNAMALLA project from UNAM, México, for their support in mesh generation over irregular regions. We also thank to anonymous referees for their valuable comments and suggestions.

References

[1] I. Abelló Ugalde, V. Hernández Mederos, P. Barrera Sánchez, G. González Flores, Injectivity of B-spline biquadratic maps, Computer Methods in Applied Mechanics and Engineering, 341, 586–608, 2018.

[2] Y. Bazilevs, L. Beirão Da Veiga, J. Cottrell, T.J.R. Hughes, G. Sangalli, Isogeometric analysis: Approximation, stability and error estimates for h-refined meshes, Mathematical Models and Methods in Applied Sciences, 16 (7), 1031-1090, 2006.

[3] Y. Bazilevs, V.M. Calo, Y. Zhang, T.J.R. Hughes, Isogeometric fluid?structure interaction analysis with applications to arterial blood flow, Computational Mechanics, 38 (4), 310-322, 2006.

[4] C. de Boor, A practical guide to splines. Springer, New York. 2001.

[5] M. Brovka, J.I. López, J.M. Escobar, R. Montenegro, J.M. Cascón, A simple strategy for defining polynomial spline spaces over hierarchical T-meshes, Computer Aided Design, 72, 140–156, 2016.

[6] A. Buffa, G. Sangalli, R. Vázquez, Isogeometric analysis in electromagnetics: B-splines approximation, Computer Methods in Applied Mechanics and Engineering, 199 (17), 1143–1152, 2010.

[7] L. Coox, E. Deckers, D. Vandepitte, W. Desmet, A performance study of NURBS-based isogeometric analysis for interior two dimensional time-harmonic acoustics, Computer Methods in Applied Mechanics and Engineering, 305, 441-467, 2016.

[8] J.A. Cottrell, T.J.R. Hughes, Y. Bazilevs, Isogeometric analysis: toward integration of CAD and FEA. John Wiley 2009.

[9] G.C. Diwan, M.S. Mohamed, Pollution studies for high order isogeometric analysis and finite element for acoustic problems, Computer Methods in Applied Mechanics and Engineering, 350, 701-718, 2019.

[10] G.C. Diwan, M.S. Mohamed, Iterative solution of Helmholtz problem with high-order isogeometric analysis and finite element method at mid-range frequencies, Computer Methods in Applied Mechanics and Engineering, 363, 112855, 2020.

[11] V. Dwarka, C. Vuik, Scalable convergence using two-level deflation preconditioning for the Helmholtz equation, SIAM Journal on Scientific Computing, 42 (2), A901-A928, 2020.

[12] V. Dwarka, R. Tielen, M. Möller, C. Vuik, Towards accuracy and scalability: Combining Isogeometric Analysis with deflation to obtain scalable convergence for the Helmholtz equation, Computer Methods in Applied Mechanics and Engineering, 377, 113694, 2021.

[13] Y.A. Erlangga, C. Vuik, C.W. Oosterlee, On a class of preconditioners for solving the Helmholtz equation, Applied Numerical Mathematics, 50 (3-4), 409-425, 2004.

[14] O.G. Ernst, M.J. Gande, Why it is Difficult to Solve Helmholtz Problems with Classical Iterative Methods, Numerical Analysis of Multiscale Problems, 325–363, 2011.

[15] A. Falini, J. Špeh, B. Jüttler, Planar domain parameterization with THB-splines, Computer Aided Geometric Design, 35, 95–108, 2015.
[16] S. Fu, K. Gao, A fast solver for the Helmholtz equation based on the generalized multiscale finite-element method, Geophysical Journal International, 211, 819-835, 2017.
[17] M.J. Gander, I.G. Graham, E.A. Spence, Applying GMRES to the Helmholtz equation with shifted Laplacian preconditioning: what is the largest shift for which wavenumber-independent convergence is guaranteed?, Numerische Mathematik, 131 (3), 567-614, 2015.
[18] M.B. van Gijzen, Y.A. Erlangga, C. Vuik, Spectral analysis of the discrete Helmholtz operator preconditioned with a shifted Laplacian, SIAM J. Sci. Comput., 29, 1942-1958, 2007.
[19] I.G. Graham, S.A. Sauter, Stability and finite element error analysis for the Helmholtz equation with variable coefficients, Mathematics of Computation, 89, 105–138, 2020.
[20] J. Gravesen, A. Evgrafov, D.M. Nguyen, P. Nortoft, Planar Parametrization in Isogeometric Analysis, Mathematical Methods for Curves and Surfaces, M. Floater et al (Ed), Springer, 189–212, 2014.
[21] T.J.R. Hughes, J. Cottrell, Y. Bazilevs, Isogeometric analysis: CAD, finite elements, NURBS, exact geometry and mesh refinement, Computer Methods in Applied Mechanics and Engineering, 194, 4135–4195, 2005.
[22] T.J.R. Hughes, A. Reali, G. Sangalli, Efficient quadrature for NURBS-based isogeometric analysis, Computer Methods in Applied Mechanics and Engineering, 199, 301-313, 2010.
[23] F. Ihlenburg, I. Babuska, Finite element solution of Helmholtz equation with high wave number. Part I: the h-version of FEM, Computers & Mathematics with Applications, 30 (9), 9–37, 1995.
[24] F. Ihlenburg, I. Babuska, Finite element solution of Helmholtz equation with high wave number. Part II: the h-p version of FEM, SIAM Journal on Numerical Analysis, 34 (1), 315-358, 1997.
[25] P.M. Knupp, Algebraic mesh quality metrics, SIAM Journal on Scientific Computing, 23 (1), 193–218, 2001.
[26] S. Lipton, J.A. Evans, Y. Bazilevs, T. Elguedj, T.J.R. Hughes, Robustness of isogeometric structural discretizations under severe mesh distortion, Computer Methods in Applied Mechanics and Engineering, 199, 357-373, 2010.
[27] J. Melenk, S. Sauter, Convergence analysis for finite element discretizations of the Helmholtz equation with Dirichlet-to-Neumann boundary conditions, Mathematics of Computation, 79 (272), 1871-1914, 2010.
[28] W.F. Mitchell, A collection of 2D elliptic problems for testing adaptive grid refinement algorithms, Applied Mathematics and Computation, 220, 350-364, 2013.
[29] A. Moiola, E. Spence, Is the Helmholtz Equation Really Sign-Indefinite?, SIAM Review, 56 (2), 274-312, 2014.
[30] T. Nguyen, B. Jüttler, Parameterization of contractible domains using sequences of harmonic maps, in: Curves and Surfaces, Springer, Berlin, Heidelberg, 501–514, 2012.
[31] X. Nian, F. Chen, Planar domain parameterization for isogeometric analysis based on Teichmüller mapping, Computer Methods in Applied Mechanics and Engineering, 311, 41–55, 2016.
[32] A.H. Sheikh, D. Lahaye, L. Garcia Ramos, R. Nabben, C. Vuik, Accelerating the Shifted Laplace Preconditioner for the Helmholtz Equation by Multilevel Deflation, Journal of Computational Physics, 322, 473–490, 2016.
[33] E.A. Spence, When all else fails, integrate by parts?- an overview of new and old variational formulations for linear elliptic PDEs in Unified Transform Method for Boundary Value Problems: Applications and Advances? A.S. Fokas and B. Pellonieds, SIAM, 2015.
[34] G. Xu, B. Mourrain, R. Duvigneau, A. Galligo, Optimal Analysis-Aware Parameterization of Computational Domain in Isogeometric Analysis, Advances in Geometric Modeling and Processing, Lecture Notes in Computer Science, 236–254, Springer, 2010.
[35] G. Xu, B. Mourrain, R. Duvigneau, A. Galligo, Parametrization of computational domain in isogeometric analysis: methods and comparison, Computer Methods in Applied Mechanics and Engineering, 200, 2021–2031, 2011.
[36] G. Xu, B. Mourrain, R. Duvigneau, A. Galligo, Constructing analysis-suitable parameterization of computational domain from CAD boundary by variational harmonic method, Journal of Computational Physics, 252, 275–289, 2013.

[37] G. Xu, M. Li, B. Mourrain, T. Rabczuk, J. Xu, S.P.A. Bordas, Constructing IGA-suitable planar parameterization from complex CAD boundary by domain partition and global/local optimization, Computer Methods in Applied Mechanics and Engineering, 328, 175–200, 2018.
[38] Y. Zhang, Y. Bazilevs, S. Goswami, C.L. Bajaj, T.J.R. Hughes, Patient-specific vascular NURBS modeling for isogeometric analysis of blood flow, Computer Methods in Applied Mechanics and Engineering, 196 (29), 2943-2959, 2007.

Instituto de Cibernética, Matemática y Física Calle E, No. 309, Vedado, La Habana, Cuba
E-mail: vicky@icimaf.cu

CEPES, Univ. de La Habana, San Lázaro y L, La Habana, Cuba
E-mail: isidro@cepes.uh.cu

Fac. de Matemática y Computación, Univ. de La Habana, San Lázaro y L, La Habana, Cuba
E-mail: rbruno2k15@gmail.com

DIAM, TU Delft, The Netherlands
E-mail: d.j.p.lahaye@tudelft.nl

Dpto. Análisis Matemático, Univ. de La Laguna, Tenerife, España.
E-mail: vguerrao@ull.edu.es